Contents lists available at ScienceDirect

Chemosphere

Technical Note

Enhanced photocatalytic activity of V_2O_5–ZnO composites for the mineralization of nitrophenols

M. Aslam [a], Iqbal M.I. Ismail [a,b], T. Almeelbi [a,c], Numan Salah [d], S. Chandrasekaran [a], A. Hameed [a,e,*]

[a] Centre of Excellence in Environmental Studies (CEES), King Abdulaziz University, Jeddah 21589, Saudi Arabia
[b] Chemistry Department, Faculty of Science, King Abdulaziz University, Jeddah 21589, Saudi Arabia
[c] Department of Environmental Sciences, King Abdulaziz University, Jeddah 21589, Saudi Arabia
[d] Center of Nanotechnology, King Abdulaziz University, Jeddah 21589, Saudi Arabia
[e] National Centre for Physics, Quaid-e-Azam University, Islamabad 44000, Pakistan

HIGHLIGHTS

- Enhanced photocatalytic activity of V_2O_5–ZnO composites for the mineralization of nitrophenols in sunlight.
- Superoxide anion radicals are the major contributors in removal of 2-NP and 2,4-DNP.
- The removal of 4-NP is mediated by hydroxyl radicals.
- V_2O_5 promotes the formation of hydroxyl radicals.
- Nitrite ions are further oxidized to NO_3^- and $ONOO^-$ anions.

GRAPHICAL ABSTRACT
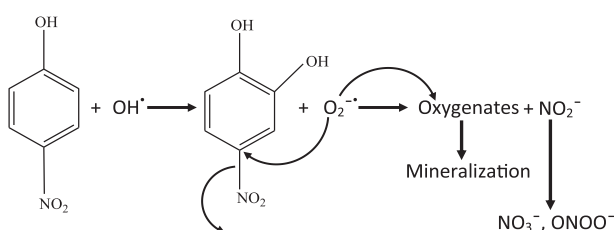
ARTICLE INFO

ABSTRACT

In an effort to enhance the photocatalytic activity of ZnO in natural sunlight, V_2O_5–ZnO nanocomposites were synthesized by co-precipitation technique. The characterization of the synthesized powders by FESEM, XRD and UV–visible diffuse reflectance spectroscopy (DRS) revealed that the both V_2O_5 and ZnO retain their individual identity in the composites but the increasing concentration of V_2O_5 affect the particle size of ZnO. As estimated by photoluminescence spectroscopy, in comparison to pure ZnO, the presence of V_2O_5 significantly suppressed the charge carrier's recombination process. The photocatalytic activity of the synthesized powders was evaluated for the degradation/mineralization of three potential nitrophenol pollutants (2-nitrophenol, 4-nitrophenol, and 2,4-dinitrophenol). The synthesized composites showed significantly higher activity for both degradation and mineralization of nitrophenols compared to pure ZnO. The progress of the degradation process was evaluated by HPLC while mineralization was monitored by TOC analysis. The degradation/mineralization route was estimated by identifying the intermediates using GC–MS. The correlation of the experimental data revealed that the position of NO_2 group in 2- and 4-nitrophenol significantly affect the rate of degradation. The identification of hydroxyl group containing intermediates in the degradation of 4-NP confirmed the formation and vital role of hydroxyl radicals in degradation process. The rapid mineralization of nitrophenol substrates pointed out superoxide anions as major contributors in degradation and mineralization process. The assessment of the release of relevant ions (NO_2^-, NO_3^-, $ONOO^-$ and NH_4^+) during the degradation process assisted in identifying the plausible interaction sites.

* Corresponding author at: Centre of Excellence in Environmental Studies (CEES), King Abdulaziz University, Jeddah 21589, Saudi Arabia. Tel.: +966 506406684.
E-mail address: afmuhammad@kau.edu.sa (A. Hameed).

1. Introduction

Nitrophenol (NP) derivatives, because of their extensive use as raw materials in chemical processing industries, are the major phenol derivatives in the industrial effluent (Andreozzi et al., 1999). The chemically stable NP resists chemical and biological removal (Tryk et al., 2000; Carey, 2000). NP derivatives are converted to chlorinated phenolic compounds during the chlorination process for the removal of microorganisms, thus generating offshoots that are more toxic (Adav et al., 2007; Gondal et al., 2009; Hayat et al., 2011a). Based on the toxicity and hazard, the maximum permissible limits of NP, especially 2-NP, 4-NP and 2,4-DNP, as established by USEPA, are less than 20 ppb (USEPA, 1980). Currently no conventional single step process is available for the complete removal of these pollutants without leaving any toxic by-products (Aksu and Yener, 2001). Among the photon-based oxidation technologies (Andreozzi et al., 1999), sunlight photocatalysis can provide an economically viable and single-step solution to this issue (Bahnemann, 2004; Kositzi et al., 2004; Malato et al., 2009). Among the existing photocatalysts, TiO$_2$ is widely studied photocatalyst in this regard but due to its wide bandgap of 3.2 eV, most of the studies are performed in UV exposure (Schiavello, 1988; Pelizzetti and Serpone, 1989; Ollis et al., 1991; Hoffmann et al., 1995; Mills and Le Hunte, 1997; Palmisano and Sclafani, 1997; Tryk et al., 2000; Aksu and Yener, 2001; Gondal et al., 2008). Sunlight, being cheap and renewable, is freely available in the nature. Therefore, the use of sunlight as a light source in photocatalysis can make these processes, even more feasible for commercial applicability. However, the non-availability of single photocatalyst fulfilling the requirements of high photon absorption and appreciable photocatalytic activity in the solar spectrum is a serious constraint on the exercise of this option. The existing most active photocatalysts such as TiO$_2$ and ZnO, due to their wide bandgap, can absorb ⩽5% of the total incident sunlight photons and therefore are not a suitable for sunlight photocatalytic applications. The choices in this contest are; either to develop new sunlight active photocatalysts having activity comparable to TiO$_2$ or ZnO in UV region or to modify the existing active photocatalysts for enhanced activity in sunlight exposure. The strategies for enhancing the photocatalytic activity of ZnO and TiO$_2$ are reviewed in detail (Rehman et al., 2009). Among the proposed techniques, composite formation is regarded as an effective tool in improving the productivity of ZnO by suppressing the unwanted electron hole pair recombination. The components of the composite support each other by the mutual transfer of charge carriers and retain their individual identity. In bi-component composites, both the components of the composite depending on their band edge can absorb photons individually, thus behaving as tandem photocatalysts (Hameed et al., 2008, 2009a,b; Hayat et al., 2011b; Ali et al., 2014).

ZnO, a n-type semiconductor with a band gap of 3.2 eV, absorbs photons in the UV region (Xu and Schoonen, 2000). Being inexpensive and non-toxic, it is regarded as a suitable choice for photocatalytic water decontamination. Owing to its better photon absorption cross-section, for particular applications, ZnO is preferred over TiO$_2$ (Bahnemann, 2004; Pardeshi and Patil, 2008; Gaya et al., 2010; Sugiyama et al., 2012) however, its stability and high recombination rate of charge carriers under illumination are the drawbacks that are needed to be addressed. V$_2$O$_5$ is visible light responsive versatile photocatalyst. V$_2$O$_5$ is slightly soluble in water that questions its suitability for water purification purposes. It has been reported that the issues of chemical stability and photocorrosion can be eliminated by composite formation (Hameed et al., 2008; Rehman et al., 2009).

The present study is an attempt to enhance the photocatalytic activity of ZnO by making its composite with V$_2$O$_5$ by co-precipitation route. The stability of the composites was monitored by ICP analysis for Zn and V in the solution before and after exposure to sunlight. The photocatalytic performance of the synthesized composites was evaluated for the degradation/mineralization of three important NP pollutants namely; 2-NP, 4-NP and 2,4-DNP in sunlight exposure. The interesting aspect of the study is that all experiments were performed in a completely natural environment without applying any conditions for controlling the parameters such as temperature, pH, pressure, stirring, and oxygen flow.

2. Experimental details

V$_2$O$_5$–ZnO composites, loaded with 1%, 3%, 5% and 10% V$_2$O$_5$ with respect to the weight of ZnO, were synthesized by dissolving the stoichiometric amounts of NH$_4$VO$_3$ (Sigma–Aldrich, 99.5%) and Zn(NO$_3$)$_2$·6H$_2$O (Sigma–Aldrich, 99.99%) in 500 mL de-ionized water. For the synthesis of 1% V$_2$O$_5$–ZnO, the metal solution containing 0.0229 g of ammonium meta-vanadate and 4.54 g of zinc nitrate was hydrolyzed with drop wise addition of 0.5 M NaOH (Panreac, 99.9%) solution with vigorous stirring and maintained the pH at 12. The gel formed was heated at 250 °C for 3 h under stirring to convert gelatinous material to yellowish precipitates. The precipitates were filtered and washed several times with de-ionized water till neutral pH of the filtrate. To ensure stoichiometry and complete precipitation, the filtrate was checked for the possible presence of V^{5+} ions in the solution. The co-precipitates were dried at 120 °C in oven, crushed to fine powder and calcined at 450 °C in a muffle furnace for 4 h. Pure ZnO was also synthesized by adopting the same procedure.

Solid-state diffuse reflectance spectra (DRS) of synthesized composites were recorded by Perkin Elmer UV–visible diffuse reflectance spectrophotometer in the 200–900 nm range. The photoluminescence (PL) spectra of the synthesized composites, in comparison to pure ZnO, were recorded by *HORIBA Scientific* (Jobin Yvon *Fluoro Log 3*), France, macro PL system. The samples were excited at 325 nm while the emission response was recorded in the 350–700 nm range. Powder XRD patterns were acquired using a Xpert X-ray powder diffractometer (Philips PW1398) with Cu Kα radiation source from 20° to 80° (2θ) with a step time of 3 s and step size of 0.05°. The crystallite sizes of different phases identified were calculated by applying the Scherrer's equation to the major reflections. The changes in the morphology of the synthesized composites, in comparison to pure ZnO, were observed by Field Emission Scanning Electron Microscope (JEOL JSM 6490-A). The chemical composition and ionic state of V$_2$O$_5$–ZnO composites were recorded in the binding energy range of 0–1100 eV using X-ray photoelectron spectroscopy (XPS, PHI 5000 VersaProbe II, ULVAC-PHI)

The photocatalytic performance of the synthesized composites, in comparison to pure ZnO, was evaluated for the degradation of 2-NP, 4-NP and 2,4-DNP in the natural sunlight exposure. A 30 ppm solution of the respective mono and dinitrophenol was used for degradation studies. In a typical experiment, 150 mL of the catalyst/substrate solution, containing 30 ppm respective NP and 100 mg of the catalyst, was exposed to sunlight in a glass reactor without stirring. The optimization of the catalyst loading was based on the minimum amount of the catalyst that furnished significant activity for degradation. The catalyst loading was adjusted for pure ZnO and kept constant for synthesized composites, for comparison. All the experiments were carried out in the fixed period of the daylight in the measured sunlight illumination of 1000 ± 100 × 10^2 lx without any temperature and pressure control. The progress of degradation process was monitored by drawing the samples after every 20 min in the 1 h and after 30 min in the next

1.5 h. The catalyst was removed by using 0.20 μm Millipore filter. The collected samples were analyzed by HPLC (SPD-20A, Shimadzu, Japan) using 60:40 methanol–water mixture as solvent and c18 column at 254 nm. Ion chromatograph, Dionex (ICS-5000+EG Eluent Generator), was used to measure concentration of released ions during the photocatalytic process. TOC-VCPH total carbon analyzer supplied by Shimadzu, Japan, measured the removal of TOC. The samples drawn after 20 min of sunlight exposure were analyzed by GC–MS (Shimadzu, Japan, Shimadzu-QP2010 Plus) equipped with RtX1 capillary column, for the identification of intermediates formed during the mineralization process. High purity (99.999%) helium gas was used as carrier. The presence of respective NP substrates in GC–MS analysis was used as a marker for the validation of procedure adopted for analysis.

3. Results and discussion

3.1.1. Characterization of V_2O_5–ZnO composites

The comparison of solid-state absorption spectra of pure ZnO and synthesized V_2O_5–ZnO composites is presented in Fig. 1, where compared to pure ZnO, the absorption of photons in the visible region increases with the increase in V_2O_5 contents that represents the absorption by the V_2O_5 portion of the synthesized composites. With the absorption of photons in ZnO, the major optical transitions arise due to the shifting of electrons from the O (2p) orbitals to Zn (3d) orbitals. Like Zn, V is also a 3d metal, therefore the main transitions in V_2O_5 correspond to the transfer of electrons from O (2p) to V (3d). Probably, owing the short V–O bond length (1.58 Å) compared to Zn–O (1.90 Å), V_2O_5 is more absorptive in the visible region than ZnO.

The comparison of PL response of pure ZnO to that of V_2O_5–ZnO composites, loaded with various percentages of V_2O_5, is presented in Fig. 2. A significant decrease in the luminescence intensity for the composite, compared to pure ZnO, illustrates that the charge carriers generated as a result of photo-excitation of ZnO is trapped by surface V_2O_5 states. Pure ZnO exhibits the characteristic bands at ∼380, ∼429 and ∼510 nm (Srikant and Clarke, 1998) that are composed of emissions due to bandgap excitations, the interstitial Zn atoms and the excitations between Zn and singly charges surface oxygen respectively (Srikant and Clarke, 1998; Willander et al., 2010). These bands, in the order of their appearance are marked as "a", "b" and "c" in Fig. 2. The significant decrease in the intensity of these bands indicates that a synergy exists between ZnO and V_2O_5 to enhance the lifetime of the excited state.
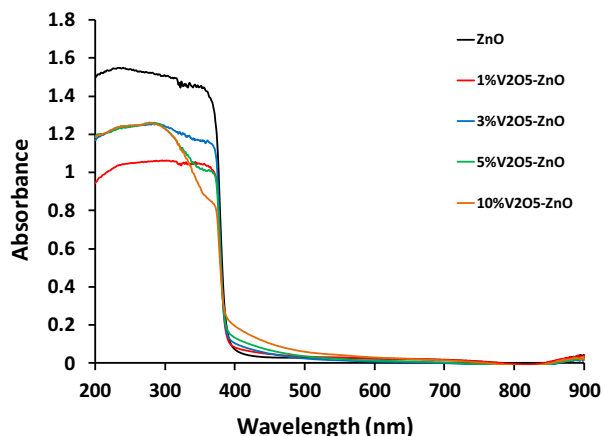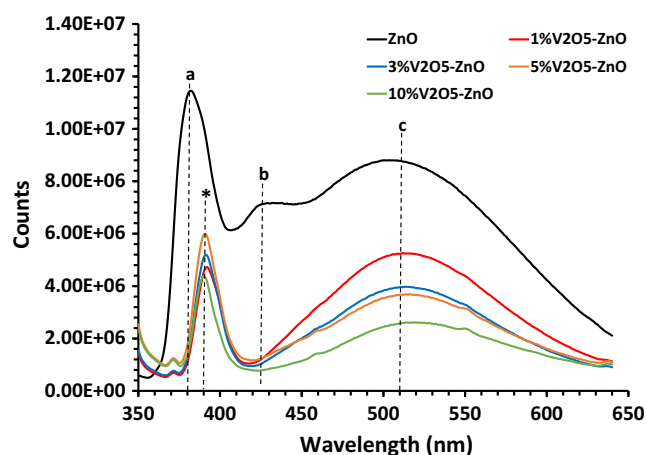

Fig. 2. The comparison of PL spectra of pure ZnO and V_2O_5–ZnO composites recorded in the range of 350–650 nm after excitation at 325 nm.

The red shift of ∼10 nm in the band at 380 nm (a) that represent the bandgap excitations in ZnO signifies that introduction of V_2O_5 states at the surface lowers that bandgap energy of ZnO either by inducing low energy surface states or by the mutual sharing of the valence band. A successive decrease with the mild red shift in the intensity of the band at 510 nm, with the increasing concentration of V_2O_5 states, indicates the diminution of free surface O⁻ sites of ZnO with the increasing occupancy of V_2O_5 entities. It is important to mention here that all the observed values for pure ZnO and V_2O_5–ZnO composites, in the PL spectra, are in agreement with the literature values (Srikant and Clarke, 1998).

The high-resolution (120,000×) FESEM images of V_2O_5–ZnO composites are presented in Fig. 3a–d. For 1% V_2O_5 loaded ZnO image, Fig. 3a, hexagonal rod shaped ZnO particles are more prominent than V_2O_5 but the presence of V_2O_5 can be identified on the surface of ZnO. From the Fig. 3b–d, the growth of V_2O_5 in various shapes is observable, however, for 10% V_2O_5–ZnO composite, the formation of needle like V_2O_5 structures (Fig. 3d) is more prominent.

The comparison of the XRD patterns of pure ZnO and synthesized V_2O_5–ZnO composites is presented in Fig. 4a. The intense reflections at 2θ values of 31, 34, 36, 47, 56, 62 and 67 matched with hexagonal, P63mc, ZnO (JCPDS 36-1451). The high intensity and sharpness of major reflections is the characteristic of phase purity and high crystallinity. The major reflections due to V_2O_5 phase were entrapped in intense ZnO reflections. The reflection at 42 and 62 were matched with orthorhombic V_2O_5 (JCPDS 41-1426). As presented in Fig. 4b, the intensity of the reflections at 42 and 62 nm, increased with the increase in V_2O_5 contents. As expected, for V_2O_5–ZnO composites, a successive decrease in the intensity of the main reflections arising due to hexagonal ZnO was also observed with the increasing concentration of V_2O_5. The average crystal size of ZnO in pure and V_2O_5–ZnO composites, evaluated by applying Scherrer's equation on the most intense reflections, varied between 35 and 60 nm while that of V_2O_5 ranged between 10.5 and 18 nm.

The comparison of XPS survey scans of the synthesized V_2O_5–ZnO composites is presented in the Supplementary Materials (Fig. S1a) where no significant shift in the binding energy of ZnO peaks was observed. The Zn 2p peaks appeared at 1020.22 eV and 1022.33 eV while O1s peak appeared at 529.9 eV. The appearance of V2p$_{3/2}$ peak at 517 eV confirmed the presence of polycrystalline V_2O_5 (Mendialdua et al., 1995). As shown in the Supplementary Materials (Fig. S1b), the increased intensity was observed with increasing V_2O_5 contents.
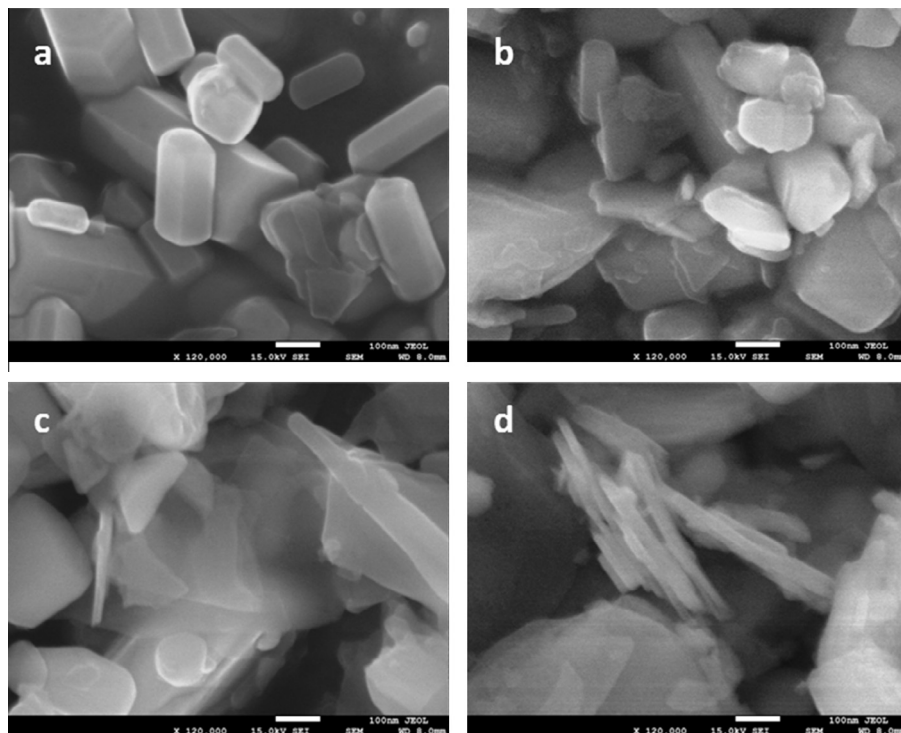

Fig. 1. The comparison of (a) the solid state absorption spectra of pure ZnO and V_2O_5–ZnO composites in 200–900 nm range.

Fig. 3. The comparison of high resolution (120,000×) SEM images of V_2O_5–ZnO composites (a) 1% V_2O_5–ZnO, (b) 3% V_2O_5–ZnO, (c) 5% V_2O_5–ZnO and (d) 10% V_2O_5–ZnO composites.
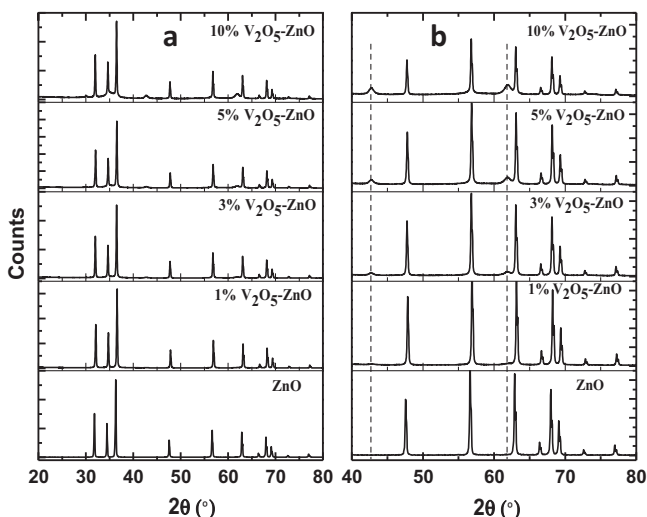

Fig. 4. The comparison XRD patterns of pure ZnO and synthesized V_2O_5–ZnO composites (a) In the range $2\theta = 20$–$80°$, (b) from $2\theta = 40$–$80°$. The dashed vertical lines indicate the reflections due to V_2O_5 phase while the unmarked reflections are due to hexagonal phase of ZnO.

3.2.2. Photocatalytic degradation of nitrophenols

In the aqueous photocatalytic system, a sequence of reactions is activated with the absorption of photons of appropriate energy ($E_p \geqslant E_g$). Both charged and radical species are generated because of water oxidation and dissolved oxygen reduction. Among the species produced, superoxide anion (O_2^{-}) and hydroxyl radicals ($HO^{\cdot}$) are the major contenders in degradation/mineralization of organic substrates. It has been proposed that the hydroxyl radicals are produced as a result of water oxidation by the photogenerated

holes (h^+) (Hoffmann et al., 1995) while the reduction of adsorbed/dissolved oxygen by excited conduction band electrons generates superoxide anions (Gaya and Abdullah, 2008; Pichat, 2013).

$$H_2O + h^+ \rightarrow H_2O^+ \rightarrow HO^{\cdot} + H^+ \tag{1}$$

$$(O_2)_{adsorbed/dissolved} + e^- \rightarrow O_2^{\cdot -} \tag{2}$$

Recently, along with the limiting the role of hydroxyl radicals in aqueous phase photocatalytic degradation process, the direct formation of these radicals by holes (h^+) oxidation (Eq. (1)) is also contradicted and a complex route based on the pH of the system has been postulated. The proposed mechanism is based on the interaction of superoxide anions ($O_2^{\cdot -}$) (Eq. (2)) with H^+ ions at low pH to form HO_2 radicals. The self-combination of HO_2 radicals leads to the formation of hydroxyl ($OH^{\cdot}$) radicals (Pichat, 2013). The proposed mechanism is outlined in the equations below.

$$O_2^{\cdot -} + H^+ \rightarrow HO_2^{\cdot} \tag{3}$$

$$HO_2^{\cdot} + HO_2^{\cdot} \rightarrow H_2O_2 + \frac{1}{2}O_2 \tag{4}$$

$$H_2O_2 + H^+ + e^- \rightarrow OH^{\cdot} + H_2O \tag{5}$$

Another alternative route, based on the oxidation of hydroxyl ions (OH^-) either produced in the system or absorbed at the surface of the catalyst, has also been proposed (Pichat, 2013).

$$OH^- + h^+ \rightarrow OH^{\cdot} \tag{6}$$

In comparison to pure ZnO, for 2-NP, the time-scale percentage degradation profiles over synthesized V_2O_5–ZnO composites in the sunlight exposure, are presented in Fig. 5a. The percentage decrease in the concentration of 2-NP with the sunlight exposure time was evaluated from the decrease in the peak heights in HPLC profiles (Supplementary Materials, Fig. S2). In the initial 20 min of exposure, for 1% V_2O_5 loaded ZnO composite, ~70% decrease in
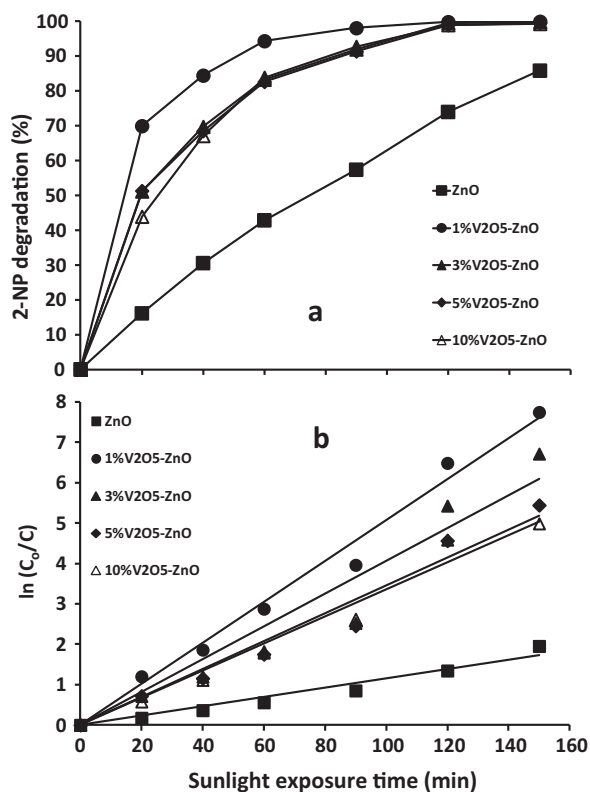
Fig. 5. The comparison of (a) time-scale percentage degradation of 2-NP (30 ppm), (b) the graphical representation of the evaluation of the rate constant "*k*" for the degradation of 2-NP in the presence of pure ZnO and synthesized V_2O_5–ZnO composites (100 mg/150 mL) in sunlight exposure (1000×10^2 LUX).

2-NP was noticed which was ~4.2 times higher than pure ZnO i.e. ~16%, in the same period. Compared to 1% V_2O_5 loaded ZnO a relatively lower activity was observed in 3%, 5% and 10% V_2O_5 loaded catalysts, however, the observed degradation of 51%, 51% and 44%, respectively, was significantly higher than pure ZnO. All the catalysts completely removed 2-NP in 150 min of exposure while in the same period, ~85% degradation of the substrate was observed over pure ZnO. The analysis of the HPLC chromatograms collected at regular intervals, as presented in the Supplementary Materials (Fig. S2), revealed that the degradation process proceeds through the formation of intermediates. Noticeably, the substrate (2-NP) and intermediates were removed simultaneously. The graphical evaluation of the rate constant "*k*" for the degradation of 2-NP over V_2O_5–ZnO composites, loaded with varying V_2O_5, is presented in Fig. 5b. The values of 0.0115 min^{-1}, 0.0507 min^{-1}, 0.0406 min^{-1}, 0.0346 min^{-1} and 0.0336 min^{-1} were evaluated for rate constant "*k*" of the degradation of 2-NP over pure, 1%, 3%, 5% and 10% V_2O_5 loaded ZnO, respectively. The comparison of the above mentioned values indicates a fivefold higher rate of degradation of 2-NP over 1% V_2O_5–ZnO composite than pure ZnO.

The degradation profile of 4-NP is presented in the Supplementary Material (Fig. S3). The degradation of 4-NP was significantly sluggish than that of 2-NP. For 1% V_2O_5–ZnO, ~60% of 4-NP substrate were removed in the initial 20 min of sunlight exposure compared to ~16% for bare ZnO in the same period. For 2-NP, ~70% removal of the substrate was observed in the same period under identical conditions. A significantly higher activity of 3% and 5% composites for 4-NP removal i.e. ~49% and ~47%, respectively, compared to pure ZnO, was also observed. However, for 10% V_2O_5 composite a distinctly lower activity was observed. The observed activity of 10% V_2O_5–ZnO was comparable to that of bare ZnO. The comparison of the HPLC profiles for the degradation of

4-NP over the composite catalysts is presented in Supplementary Materials (Fig. S4). Similar to 2-NP, the degradation of 4-NP also proceeds through the formation of intermediates, however unlike 2-NP the accumulation of the intermediates instead of simultaneous removal of intermediates and substrate was observed. Among the synthesized catalysts, only 1% V_2O_5–ZnO showed the ability to remove 4-NP completely in 150 min of sunlight exposure. The calculated values of rate constant "*k*" for of the degradation of 4-NP in the aqueous suspension of pure 1%, 3%, 5% and 10% V_2O_5 loaded ZnO were 0.0095 min^{-1}, 0.0312 min^{-1}, 0.0244 min^{-1}, 0.0212 min^{-1} and 0.0118 min^{-1}, respectively. Compared to 2-NP a marked decrease in the rate of degradation of 4-NP especially with the increasing V_2O_5 loading was noticed.

An efficient removal of 2,4-DNP over synthesized V_2O_5–ZnO composites was observable however, similar to 2-NP and 4-NP removal, a decreasing trend in the activity, with the increasing V_2O_5 loading, was perceived. The time scale percentage degradation of 2,4-DNP on the synthesized catalysts, in comparison to pure ZnO and the comparison of HPLC profiles for the degradation of 2,4-DNP over the composite catalysts are presented in Supplementary Materials (Figs. S5 and S6), respectively. The degradation of DNP substrate over 1% V_2O_5–ZnO i.e. ~68% was comparable to that of 2-NP but significantly higher than 4-NP and complete removal was observed in 150 min of sunlight exposure. For the catalysts bearing 3%, 5% and 10% V_2O_5, ~99%, 98% and 93% removal of 2,4-DNP was observed in the same period. The observed rate constants for pure ZnO and composites, with respect to the increasing concentration of V_2O_5, were 0.0056 min^{-1}, 0.0348 min^{-1}, 0.0308 min^{-1}, 0.0269 min^{-1} and 0.0182 min^{-1}, respectively. The rate constants were comparable to that observed for 2-NP and much higher than that of 4-NP. Noticeably the rate constant for the degradation of 2,4-DNP over pure ZnO was significantly lower than 2NP- and 4-NP.

The comparison of the degradation of NP substrates over 1% V_2O_5–ZnO, the most active among the synthesized composites, is presented in Supplementary Materials (Fig. S7). The observed order of degradation for the NP derivatives was: 2-NP > 2,4-DNP > 4-NP.

A trend similar to that of degradation was observed in the mineralization (removal of total organic carbon) of 2-NP, 4-NP and 2,4-DNP. The observed mineralization of 2-NP was much faster than 4-NP and 2,4-DNP. Although the mineralization of 2,4-DNP was lower than 2-NP but significantly higher than 4-NP. The comparison of the mineralization of NP substrates over 1% V_2O_5–ZnO is presented in Fig. 6a. The observed percentage mineralization for 2-NP, 4-NP and 2,4-DNP was ~95%, ~61% and ~83%, respectively. The calculated rate constants for the mineralization process of 2-NP, 4-NP and 2,4-DNP (Fig. 6b) were 0.0184 min^{-1}, 0.0119 min^{-1} and 0.0066 min^{-1}, respectively.

The comparison of the Figs. 6 and S7 revealed a significantly higher degradation of NP substrates compared to mineralization, which depicts that the substrates are degraded initially and mineralized later. A faster rate of mineralization can also be observed with decreasing concentration of NP substrates. The population of oxidizing species generated with the absorption of equal number of photons remains the same under similar reaction condition. Initially the majority of the oxidizing species interact with substrates that either result in the loss of aromaticity (cleavage of ring structure) or change in the chemical nature with the attachment of additional substituents to form "*intermediates*". Both of these situations lead to the "*degradation*" of the substrate. With the co-existence of substrates in higher and intermediates in low concentration the majority of oxidizing species interact with the substrate giving rise to higher degradation as compared to mineralization. The decreasing concentration of substrates results in the enhanced interaction of intermediates and oxidizing species that result in enhanced mineralization at later stage.
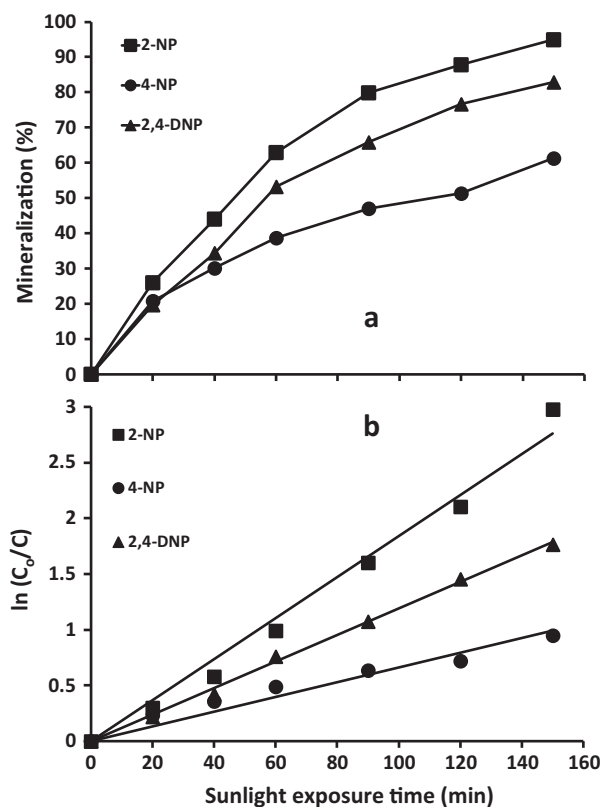
Fig. 6. The comparison of (a) percentage TOC removal (mineralization) (b) graphical evaluation of the rate constants for mineralization of 2-NP, 4-NP and 2,4-DNP (30 ppm) in the presence of 1% V_2O_5–ZnO composite (100 mg/150 mL) in sunlight exposure (1000×10^2 LUX).

The significantly high degradation and mineralization ability of the synthesized V_2O_5–ZnO composites renders that a mutual synergy exists between the two components of the composites that suppresses the recombination of charge carriers, one of the major drawbacks of ZnO, and results in the enhanced production of oxidizing species. The enhanced lifetime of the excited states is also evident in the PL analysis of the synthesized composites (Fig. 2). As apparent from DRS spectra of the synthesized composites, the two components of the composite, i.e. V_2O_5 and ZnO retain their individual identity, however, their individual bandgaps are shifted towards lower values, which is in accordance with the literature (Rehman et al., 2009). V_2O_5 is a p-type semiconductor with the band edge potentials at +3.0 V and +0.2 V in aqueous medium while ZnO is a n-type material with valance and conduction band potentials at +2.89 V and −0.31 V, respectively (Xu and Schoonen, 2000). The band edge positions of ZnO are highly suitable for the splitting of water and the reduction of dissolved oxygen to form superoxide anion radicals. On the other hand, V_2O_5 can split water but unable to reduce dissolved O_2. As per observation mentioned regarding the degradation of NP substrates, the activity of the composites decreases with increasing V_2O_5 contents. The optimum activity was observed for the composite having only 1% V_2O_5 contents. As explained in Scheme 1, by considering the positions of the band edges of the two semiconductors, it can be revealed that the only energetically favored process that can enhance the efficiency by suppressing the recombination of charge carriers, when ZnO absorbs the photons, is the trapping of photogenerated electrons by V_2O_5 surface states. It is predicted that the low surface population of V_2O_5 ($\leqslant$1.0%) induces the defects at the surface of ZnO that serve as a trap and transfer centers for the photo-excited electrons. The electron transfer ability of V_2O_5

states is affected with the increasing population that results in low activity.

Another possible reason for the decreased activity of 3% and 5% V_2O_5 loaded ZnO composites is the independent absorption of incident photons by V_2O_5 entities. For 10% V_2O_5 loading, probably the density of V_2O_5 surface states is sufficient to behave as independent catalyst. In case of photon absorption by V_2O_5 particles, the transfer of photogenerated holes (h^+) from the valence band of V_2O_5 to that of ZnO serve as a tool to suppress the $e^-–h^+$ recombination process.

As presented in HPLC and TOC profiles, the significantly higher rates of degradation as well as mineralization signifies superoxide anion radicals (O_2^-) as major contributors in both the processes. The observations in the previous studies (Lathasree et al., 2001; Bahnemann et al., 2007; Ahmed et al., 2010) also validate the major involvement of superoxide anions. The mineralization by hydroxyl radicals interaction proceeds through a number of intermediates, the high mineralization as observed in the present case is not achievable by the interaction of hydroxyl radicals (OH·) only. The identification of the intermediates formed after 30 min of sunlight exposure by GC–MS analysis further expounded the nature of oxidizing species involved in both degradation and mineralization of NP substrates. In the degradation studies with 2-NP and 2,4-DNP, no aromatic compound with or without NO_2 group, except the substrate under study, was identified, whereas in the degradation of 4-NP, along with the identification of 4-NP substrate, hydroxy NPs were identified in the appreciable concentration. The presence of this compound was also witnessed in the HPLC degradation profile of 4-NP. Therefore, it can be anticipated that 4-NP is initially converted to hydroxylated intermediates which are further attacked by the superoxide anions leading to its complete mineralization while 2-NP and 2,4-DNP are directly interacting by superoxide anions that results in the formation of open chain oxygenates like esters and carboxylic acids. These oxygenates are further engaged by the superoxide anions for complete mineralization. However, under similar experimental conditions, the formation of hydroxyl intermediates by the interaction of OH·, in the degradation of 2-NP and 2,4-DNP, cannot be completely ignored. Perhaps the rate of mineralization by the superoxide anion radicals is fast enough to identify the hydroxylated intermediates. Although a low rate of degradation as well as mineralization of NP substrates was observed in the presence of pure ZnO, no hydroxylated intermediate was observed in GC–MS or HPLC analysis that led to the conclusion that V_2O_5 promotes the generation of hydroxyl radicals. To verify the increased generation of hydroxyl radicals the pH changes of catalysts/NPs suspensions, in the dark and during the course of photocatalytic degradation experiments, were measured. With the increasing V_2O_5 contents, a significant decrease in the pH was observed with the addition of V_2O_5–ZnO composites to NP solutions in the dark. The decrease in pH was further escalated in sunlight exposure. For pure ZnO, the pH of NP solutions ranged between 7.4 and 7.8 in the dark and increased to 8.2–8.5 in the sunlight exposure with different NP substrates. During the photocatalytic degradation experiments with 10% V_2O_5–ZnO composite, the pH of the solution was dropped to 5. The decreasing trend in pH was also observed for 3% and 5% V_2O_5 loaded composites. For 1% V_2O_5 loaded ZnO, although no sharp decrease in the pH was observed, however the pH changed between 7.0 and 7.5. These observations strengthen the view that with the decrease in pH of the medium, the formation of hydroxyl radicals by the route proposed in Eqs. (3)–(5) is probable, whereas at higher pH values the hydroxyl radicals are generated by reaction mentioned in Eq. (6).

The variation in the rate of degradation and mineralization of 2NP- and 4-NP was surprising. Both isomers have comparable physical properties and the only difference between the two is
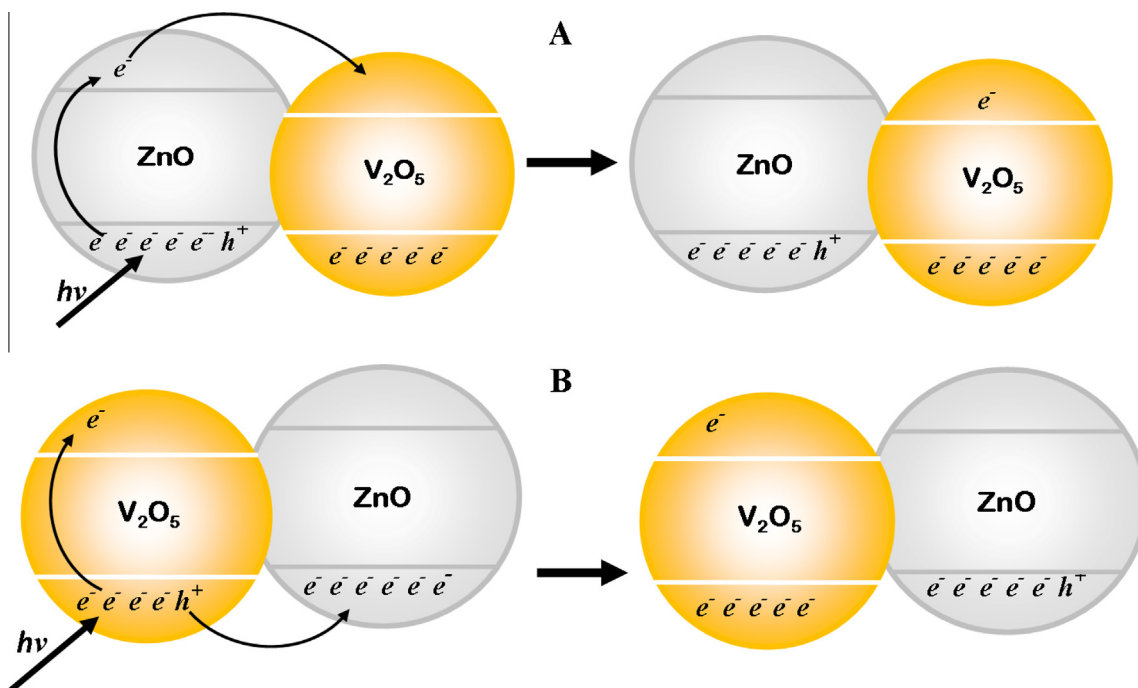
Scheme 1. The possible mechanism of carrier charge suppression in V_2O_5–ZnO composites (A) when the light is absorbed by ZnO, the photogenerated electrons (e^-) are transferred to the conduction band of V_2O_5 (B) when the light is absorbed by V_2O_5, the photogenerated holes (h^+) are transferred to the valence band of ZnO.

the position of attachment of the NO_2 group to the aromatic ring. The presence of NO_2 and OH groups on the adjacent carbon atoms and due to the possible existence of hydrogen bonding and inductive ($-I$) effect in 2-NP, the electron cloud is largely concentrated on the OH and NO_2 group bearing carbon atoms and less distributed on the aromatic ring. Conversely, in 4-NP, due to the attachment of OH and NO_2 groups on C_1 and C_4 position, opposite to each other, the electronic charge is distributed all over the ring thus imparting additional negative charge on the ring. In NPs, the electronegative oxygen atoms of NO_2 group additionally distort the electronic cloud that induces a partial positive charge on the attached carbon atom thus generating a center for the attack of negative species. This effect is more pronounced in 2-NP compared to 4-NP where the excess negative charge on the ring reduces the induced partial positive charge. Therefore, it can be estimated that the rapid degradation of 2-NP and 2,4-DNP is due to the presence of NO_2 groups induced positive centers that serve as interacting sites for the incoming negatively charged superoxide anion radicals. The displacement of the NO_2 groups as nitrite ion, the incorporation of $O_2^{·-}$ and simultaneous ring opening degrade the 2-NP substrate with the loss of aromaticity. The incorporation of electronegative oxygen in the chain induces the polarity in the intermediate compound/s that creates additional centers for $O_2^{·-}$ interaction. The $O_2^{·-}$ radicals interact with the polar intermediates that leads to the complete mineralization. For 4-NP, the excessive negative charge on the ring repels the incoming charged anions ($O_2^{·-}$) and initially transformed to hydroxylated intermediates by the interaction of uncharged hydroxyl radicals. With the substitution of OH$^·$ on the aromatic ring, having electronegative oxygen, the electron cloud is partially distorted. The hydroxylated intermediates are successively attacked by superoxide anions for degradation initially and mineralization finally as presented in Scheme 2. The hydroxyl radicals do interact with 2-NP and 2,4-DNP, however the rapid mineralization by the superoxide anions restrict their concentration to be detectable in solution.

The comparison of time dependent release of NO_2^- ions during the degradation/mineralization of 2-NP, 4-NP and 2,4-DNP, as
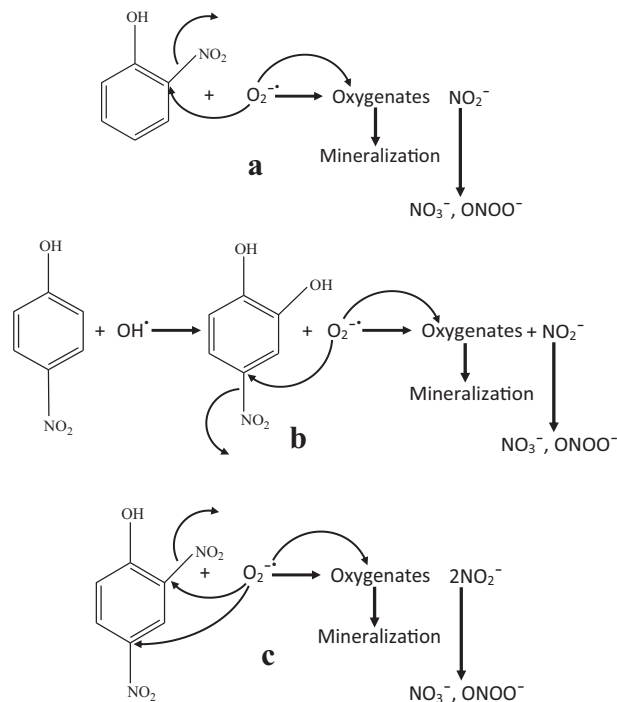
Scheme 2. Mechanism of degradation/mineralization (a) 2-NP, (b) 4-NP and (c) 2,4-DNP.

measured by ion chromatography, is presented in Fig. 7a. The release of NO_2^- ions in the solution verified the major involvement of charged $O_2^{·-}$ anions rather than neutral radical species in the degradation/mineralization process. The absence of any NO_2 containing intermediate either aromatic or aliphatic further supported the view that NO_2 groups are the first to be displaced by superoxide anions followed by the degradation of 2-NP and 2,4-DNP. A similar mechanism was anticipated in the degradation of 4-NP,
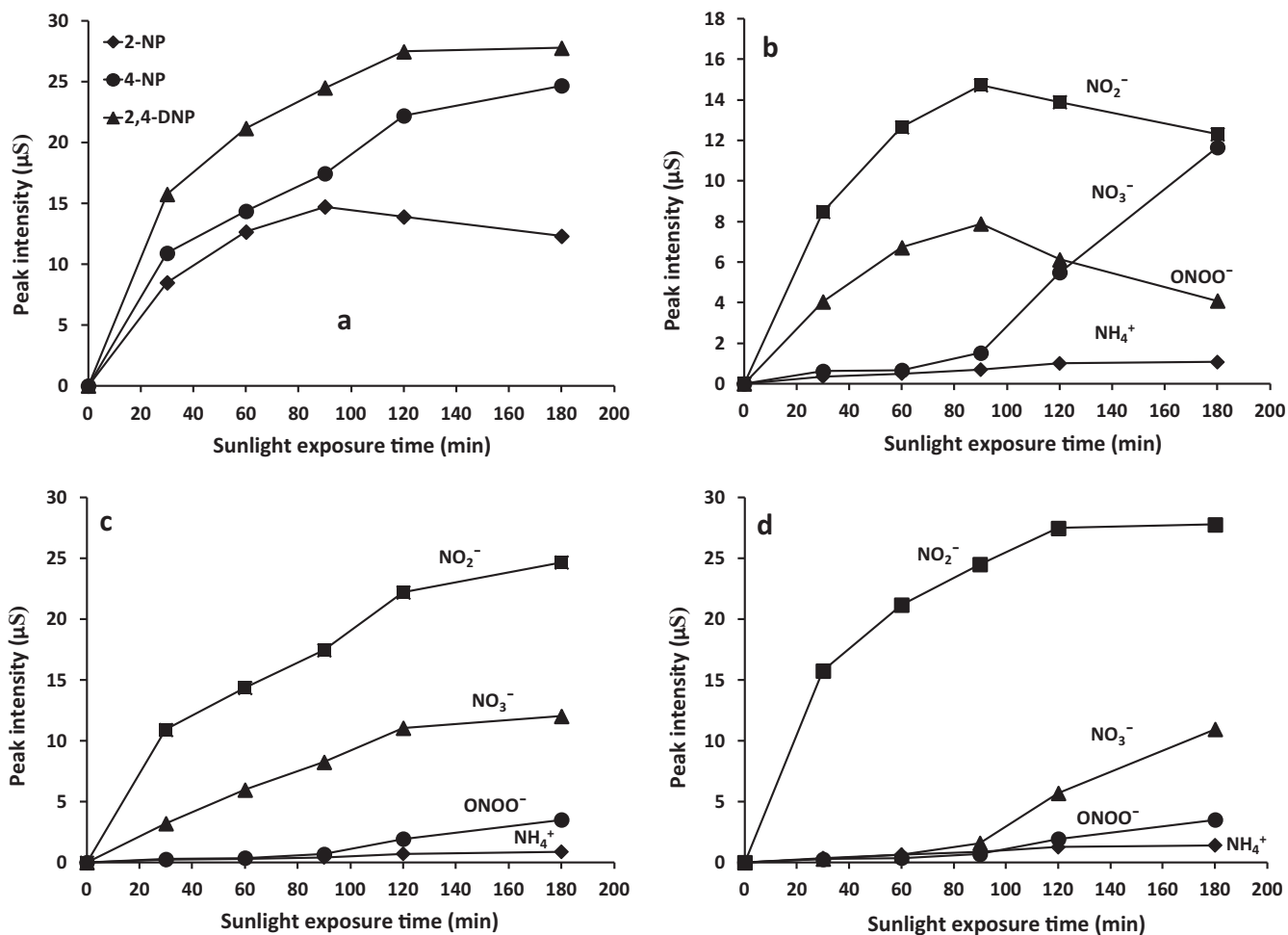
Fig. 7. The comparison of (a) release of NO_2^- ions in the degradation of 2,4-NP and 2,4-DNP (30 ppm); The pattern of the release of anions and cations identified by Ion chromatography in the degradation of, (b) 2-NP, (c) 4-NP and (d) 2,4-DNP over 1% V_2O_5–ZnO composite (100 mg/150 mL) in sunlight exposure (1000×10^2 LUX).

where the formation of hydroxylated intermediate facilitates the displacement of NO_2 groups by distorting the electron cloud. For 2-NP and 2,4-DNP the concentration of NO_2^- ions increased initially followed by a decrease. This trend led to the conclusion that NO_2^- ions after their release further interact with the oxidizing species present in the system and transformed to other anions. For 4-NP, an increasing trend with the exposure time was observed. Probably, due to the stability and the distribution of electronic cloud in 4-NP, the oxidizing species are mainly engaged in its degradation rather than interaction with NO_2^- ions. To verify this assumption all the possible ions that included NO_2^-, NO_3^-, $ONOO^-$ and NH_4^+ were estimated in the degradation of 2-NP, 4-NP and 2,4-DNP and presented in Fig. 7b–d, respectively.

Owing to the fast degradation/mineralization of 2-NP, the majority of NO_2^- ions that are released into the solution are converted to NO_3^- ions after interacting with superoxide anion radicals. The further interaction NO_3^- leads to the formation of peroxynitrite ($ONOO^-$) ions. A mild reduction of NO_2^- to NH_4^+ was also observed. All the above mentioned ions were also observed in the degradation/mineralization of 4-NP however the low yield of NO_3^- ions compared to that observed for 2-NP indicated the non-availability of O_2^- radicals for oxidation. Accordingly a low yield of peroxynitrite ($ONOO^-$) ions was also observed. Also, compared to 2-NP, a low formation of NH_4^+ ions was observed. The formation of all the above mentioned anions was also observed in the degradation/mineralization of 2,4-DNP. Having two NO_2 groups, the yield of NO_2^- ions was approximately twice than that of 2-NP. The comparison

of the IC profiles for the degradation of 2-NP, 4-NP and 2,4-DNP over 1% V_2O_5–ZnO is presented in Supplementary Materials (Fig. S8).

The composites showed excellent stability in sunlight exposure and no release of either Zn or V was observed in the ICP analysis. Additionally, no significant loss in the activity of the composites was observed in the repeated exposures.

In summary, the absence of any aromatic intermediate formed by the interaction of hydroxyl radicals, the identification of open chain oxygenated intermediates and the release of NO_2^- ions in solution confirmed that the degradation of 2-NP and 2,4-DNP is initiated by the displacement of NO_2 groups, ring opening and incorporation of oxygen in the chain. The presence of oxygen, being electronegative, imparts polarity to the molecule, thus creating sites for the superoxide anions interaction. The identification of the products ranging from C_1–C_5 oxygenates also verifies that the mineralization of the NP is not a single step process but after the ring penning smaller fragments are formed. The smaller fragments are further interacted until complete mineralization.

4. Conclusions

Composite formation has proved to be a viable tool for suppressing the recombination of charge carriers. The study proved that by applying suitable modification the photocatalytic activity of the existing active photocatalysts such as ZnO can be enhanced. In the degradation of NPs, the study confirmed the generation of hydroxyl radicals, however, their contribution is minor

in degradation/mineralization process. Superoxide anion radicals (O_2^-) are the major contributors, both in the degradation and mineralization process. The interaction of hydroxyl radicals facilitates the transformation of 4-NP molecules for superoxide anion radical's interaction. The degradation of NPs proceeds with the removal of NO_2 group, ring opening and incorporation of oxygen. The mineralization is a multistep process and the larger molecules are fragmented into smaller molecules till complete mineralization. The nitrite ions released as a consequence of superoxide anion interaction are further oxidized to NO_3^- and $ONOO^-$ anions.

Acknowledgments

Appendix A. Supplementary material

Supplementary data associated with this article can be found, in the online version, at http://dx.doi.org/10.1016/j.chemosphere.2014.05.076.

References

Adav, S.S., Chen, M.Y., Lee, D.J., Ren, N.Q., 2007. Degradation of phenol by Acinetobacter strain isolated from aerobic granules. Chemosphere 67, 1566–1572.

Ahmed, S., Rasul, M.G., Martens, W.N., Brown, R.J., Hashib, M.A., 2010. Heterogeneous photocatalytic degradation of phenols in wastewater: a review on current status and developments. Desalination 261, 3–18.

Aksu, Z., Yener, J., 2001. A comparative adsorption/biosorption study of monochlorinated phenols onto various sorbents. Waste Manage. 21, 695–702.

Ali, Z., Aslam, M., Ismail, I.M.I., Hameed, A., Hussain, S.T., Chaudhry, M.N., Gondal, M.A., 2014. Synthesis, characterization and photocatalytic activity of Al_2O_3–TiO_2 based composites. J. Environ. Sci. Health A 49, 1–11.

Andreozzi, R., Caprio, V., Insola, A., Marotta, R., 1999. Advanced oxidation processes (AOP) for water purification and recovery. Catal Today 53, 51–59.

Bahnemann, D., 2004. Photocatalytic water treatment: solar energy applications. Sol. Energy 77, 445–459.

Bahnemann, W., Muneer, M., Haque, M.M., 2007. Titanium dioxide-mediated photocatalysed degradation of few selected organic pollutants in aqueous suspensions. Catal. Today 124, 133–148.

Carey, F.A., 2000. Organic Chemistry, fourth ed. McGraw-Hill, New York. p. 945.

Gaya, U.I., Abdullah, A.H., 2008. Heterogeneous photocatalytic degradation of organic contaminants over titanium dioxide: a review of fundamentals, progress and problems. J. Photochem. Photobiol. C Photochem. Rev. 9, 1–12.

Gaya, U.I., Abdullah, A.H., Zainal, Z., Hussein, M.Z., 2010. Photocatalytic degradation of 2,4-dichlorophenol in irradiated aqueous ZnO suspension. Int. J. Chem. 2, 180–189.

Gondal, M.A., Sayeed, M.N., Seddighi, Z., 2008. Laser enhanced photo-catalytic removal of phenol from water using p-type NiO semiconductor catalyst. J. Hazard. Mater. 155, 83–89.

Gondal, M.A., Sayeed, M.N., Yamani, Z.H., Arfaj, A., 2009. Efficient removal of phenol from water using Fe2O3 semiconductor catalyst under UV laser irradiation. J. Environ. Sci. Health A 44, 515–521.

Hameed, A., Montini, T., Gombac, V., Fornasiero, P., 2008. Surface phases and photocatalytic activity correlation of Bi_2O_3/Bi_2O_{4-x} nanocomposites. J. Am. Chem. Soc. 130, 9658–9659.

Hameed, A., Montini, T., Gombac, V., Fornasiero, P., 2009a. Photocatalytic decolourization of dyes on NiO–ZnO nano-composites. Photochem. Photobiol. Sci. 8, 677–682.

Hameed, A., Gombac, V., Montini, T., Graziani, M., Fornasiero, P., 2009b. Synthesis, characterization and photocatalytic activity of NiO–Bi_2O_3 nano-composites. Chem. Phys. Lett. 472, 212–216.

Hayat, K., Gondal, M.A., Khaled, M.M., Ahmed, S., 2011a. Effect of operational key parameters on photocatalytic degradation of phenol using nanonickel oxide synthesized by sol–gel method. J. Mol. Catal. A 336, 64–71.

Hayat, K., Gondal, M.A., Khaled, M.M., Ahmed, S., Shemsi, A.M., 2011b. Nano ZnO synthesis by modified sol gel method and its application in heterogeneous photo-catalysis removal of phenol from water. Appl. Catal. A 393, 122–129.

Hoffmann, M.R., Martin, S., Choi, W., Bahnemann, D.W., 1995. Environmental applications of semiconductor photocatalysis. Chem. Rev. 95, 69–96.

Kositzi, M., Poulios, I., Malato, S., Caceres, J., Campos, A., 2004. Solar photocatalytic treatment of synthetic municipal wastewater. Water Res. 38, 1147–1154.

Lathasree, S., Nageswara Rao, A., Siva Sankar, B., Sadasivam, V., Rengaraj, K., 2001. Heterogeneous photocatalytic mineralization of phenols in aqueous solutions. J. Mol. Catal. A 223, 101–105.

Malato, S., Fernández-Ibáñez, P., Maldonado, M.I., Blanco, J., Gernjak, W., 2009. Decontamination and disinfection of water by solar photocatalysis: recent overview and trends. Catal. Today 147, 1–59.

Mendialdua, J., Casanova, R., Barbaux, Y., 1995. XPS studies of V_2O_5, V_6O_{13}, VO_2 and V_2O_3. J. Electron Spectrosc. Relat. Phenom. 71, 249–261.

Mills, A., Le Hunte, S., 1997. An overview of semiconductor photocatalysis. J. Photochem. Photobiol., A 108, 1–35.

Ollis, D.F., Pelizzetti, E., Serpone, N., 1991. Photocatalyzed destruction of water contaminants. Environ. Sci. Technol. 25, 1522–1529.

Palmisano, L., Sclafani, A., 1997. In heterogeneous photocatalysis. In: Schiavello, M. (Ed.), Wiley Series: Photoscience and Photoengineering, vol. 3. John Wiley, Chichester, p. 109.

Pardeshi, S.K., Patil, A.B., 2008. A simple route for photocatalytic degradation of phenol in aqueous zinc oxide suspension using solar energy. Sol. Energy 82, 700–705.

Pelizzetti, E., Serpone, N. (Eds.), 1989. Photocatalysis: Fundamentals and Applications. Wiley, New York, USA.

Pichat, P., 2013. Photocatalysis and Water Purification: From Fundamentals to Recent Applications, first ed. Wiley-VCH Verlag, Weinheim, Germany.

Rehman, S., Ullah, R., Butt, A.M., Gohar, N.D., 2009. Strategies of making TiO_2 and ZnO visible light active. J. Hazard. Mater. 170, 560–569.

Schiavello, M., 1988. Photocatalysis and Environment: Trends and Applications. Kluwer Academic Publishers, Dordrecht, The Netherlands.

Srikant, V., Clarke, D.R., 1998. On the optical band gap of zinc oxide. J. Appl. Phys. 83, 5447–5451.

Sugiyama, M., Salehi, Z., Tokumura, M., Kawase, Y., 2012. Photocatalytic degradation of p-nitrophenol by zinc oxide particles. Water Sci. Technol. 65, 1882–1886.

Tryk, D.A., Fujishima, A., Honda, K., 2000. Recent topics in photoelectrochemistry: achievements and future prospects. Electrochim. Acta 45, 2363–2376.

US Environmental Protection Agency, 1980. Ambient Water Quality Criteria for Nitrophenols, Washington, DC.

Willander, M., Nur, O., Sadaf, J.R., Qadir, M.I., Zaman, S., Zainelabdin, A., Bano, N., Hussain, I., 2010. Luminescence from zinc oxide nanostructures and polymers and their hybrid devices. Materials 3, 2643–2667.

Xu, Y., Schoonen, M.A.A., 2000. The absolute energy positions of conduction and valence bands of selected semiconducting minerals. Am. Min. 85, 543–556.